Article

Skeletal CH$_3$OH/NO$_x$ Kinetic Model for Simulating Spark-Ignition and Turbulent Jet Ignition Engines

Wenxian Tang,* Mickael Silva, Khaiyom Hakimov, Xiaoyuan Zhang, Ponnya Hlaing, Emre Cenker, Abdullah S. AlRamadan, James W. G. Turner, Aamir Farooq, Hong G. Im, and S. Mani Sarathy

Cite This: ACS Omega 2024, 9, 11255−11265

Read Online

ACCESS | Metrics & More | Article Recommendations | SI Supporting Information

ABSTRACT: Methanol is a promising renewable fuel for achieving a better engine combustion efficiency and lower exhaust emissions. Under exhaust gas recirculation conditions, trace amounts of nitrogen oxides have been shown to participate in fuel oxidation and impact the ignition characteristics significantly. Despite numerous studies that analyzed the methanol/NO$_x$ interaction, no reliable skeletal kinetic mechanism is available for computational fluid dynamics (CFD) modeling. This work focuses on developing a skeletal CH$_3$OH/NO$_x$ kinetic model consisting of 25 species and 55 irreversible and 27 reversible reactions, used for full-cycle engine combustion simulations. New experiments of methanol with the presence of 200 ppmv NO/NO$_2$ were conducted in a rapid compression machine (RCM) at engine-relevant conditions (20−30 bar, 850−950 K). Experimental results indicate notable enhancement effects of the presence of NO/NO$_2$ on methanol ignition under the conditions tested, which highlights the importance of including the CH$_3$OH/NO$_x$ interactions in predicting combustion performance. The proposed skeletal mechanism was validated against the literature and new methanol and methanol/NO$_x$ experiments over a wide range of operating conditions. Furthermore, the skeletal mechanism was applied in three-dimensional (3D) CFD full-cycle simulations of spark-ignition (SI) and turbulent jet ignition (TJI) engine combustion using methanol. Simulation results demonstrate good agreement with experimental measurements of pressure traces and engine metrics, proving that the proposed skeletal mechanism is suitable and sufficient for CFD simulations.
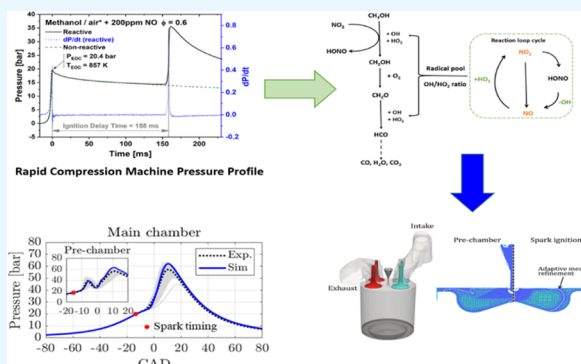
1. INTRODUCTION

Methanol (CH$_3$OH) is a promising sustainable fuel that can be produced from low-carbon-intensity pathways, including biomass or hydrogen/carbon dioxide feedstock.[1,2] Moreover, methanol has a higher octane number and lower carbon content compared to gasoline, making it a potential fuel in engines. The application of methanol in engines can enhance combustion efficiency and lower exhaust emissions, such as nitrogen oxides (NO$_x$) and particulate matter.[3−5] Along with fuel selection, exhaust gas recirculation (EGR) has been extensively employed as an effective pretreatment in various combustion engines to reduce and control NO$_x$ emissions, as well as improve engine thermal efficiency and control combustion phasing.[6−8]

The combustion of hydrocarbon fuels typically generates exhaust gases comprising various components, such as nitrogen (N$_2$), carbon dioxide (CO$_2$), and water vapor (H$_2$O), as well as unburned hydrocarbons and nitrogen oxides (NO, NO$_2$).[9] EGR recirculates a portion of the exhaust gas back into the engine intake, which can alter the composition of the air/fuel mixture, thus resulting in a complex impact on engine combustion performance. Dilution gases, such as N$_2$, H$_2$O, and CO$_2$, can contribute to reducing the NO$_x$ emission by lowering the flame temperature and decreasing the O$_2$ concentration in combustion systems, as NO$_x$ formation is favored at high temperatures and oxygen-rich conditions.[6−8] However, dilution can also alter the thermophysical properties of the reacting mixture, thus affecting the oxidation reaction kinetics.[10] Few studies[10−12] have examined the effects of main constituents of residual gas (N$_2$, CO$_2$, H$_2$O) on premixed methanol/air flames at various conditions. Their findings suggest that the chemical effects of these components were negligible, while thermal effects played a dominant role.

Among EGR species, trace amounts of NO and NO$_2$ are known to participate in fuel oxidation and impact ignition characteristics. The effects of these species depend on various factors, including the temperature−pressure regimes, equivalence ratios, and the amounts of NO/NO$_2$ present.[11,13−17] From previous studies, Koda et al.[11] showed that NO$_2$ addition

decreased ignition temperatures in a premixed methanol/air mixture in a heated quartz tube. Further research by Hjuler et al.[13] and Lyon et al.[14] found that methanol has a high potential for oxidizing NO in flow reactors at atmospheric pressure. Alzueta et al.[15] conducted experimental studies on methanol/NO interaction in a flow reactor over a wide range of equivalence ratios, showing that NO sensitizes methanol oxidation under ultralean conditions while inhibiting it in rich conditions. Moréac et al.[16] investigated the impact of different amounts of NO presence on methanol oxidation in a jet-stirred reactor (JSR) at a higher pressure of 10 atm, finding that higher amounts of NO addition further accelerated methanol oxidation compared to lower amounts. In addition, Dayma et al.[17] conducted experiments on methanol oxidation in the presence of NO and NO_2, observing that the oxidation of methanol was significantly sensitized by NO_2, whereas the effect of NO was more limited.

Despite numerous studies on CH_3OH/NO_x interactions, limited experimental work has been conducted to investigate the effects of NO_x on the methanol ignition behavior under engine combustion conditions. In this work, we conducted new experiments using a rapid compression machine (RCM) to investigate the chemical effects of NO/NO_2 additions on methanol ignition performance at engine-relevant conditions (20–30 bar, 850–950 K). Detailed kinetic mechanisms for CH_3OH and CH_3OH/NO_x combustion have been extensively studied and validated against the existing experimental data. However, these detailed mechanisms are computationally expensive and not practical for computational fluid dynamics (CFD) simulations of methanol combustion in real engine applications. Therefore, this study aims to propose a skeletal CH_3OH/NO_x kinetic model with a small size for CFD applications in full-cycle engine combustion. The proposed skeletal CH_3OH/NO_x model was validated against new and literature experiments of methanol and methanol/NO_x interactions over a wide range of temperatures, pressures, and equivalence ratios. Furthermore, the proposed skeletal model was assessed in the CFD application of spark-ignition (SI) and turbulent jet ignition (TJI) engine combustion using methanol to prove its applicability.

2. METHODS

2.1. RCM Experimental Method. Measurements of ignition delay times for CH_3OH/air mixtures with 200 ppmv NO/NO_2 were conducted in the KAUST RCM facility for the temperature range from 850 to 950 K at high pressures of 20 and 30 bar in lean ($\Phi = 0.6$) and stoichiometric ($\Phi = 1$) conditions. A detailed description of the facility was shown in previous studies.[18,19] The representative pressure–time history of the KAUST RCM is shown in Figure 1. Ignition delay time is defined as a time interval between the end of compression (EOC) and the maximum gradient pressure $(dP/dt)_{max}$ point. Experimental points were repeated to confirm the reproducibility of IDTs within 10%, followed by a nonreactive experiment, which was used to generate the volume–time history. In-chamber mixture preparation was implemented for $CH_3OH/NO/air$ mixtures. First, the $CH_3OH/NO/N_2$ mixture was prepared in heated mixing, and 5 min prior to the experiment was mixed in the combustion chamber with O_2. More details about the mixture preparation with NO can be found elsewhere.[20] MKS pressure transducers (100 and 10,000 Torr) with accuracies of 0.5% from the reading were used to read the pressures for mixture preparation. The combustion
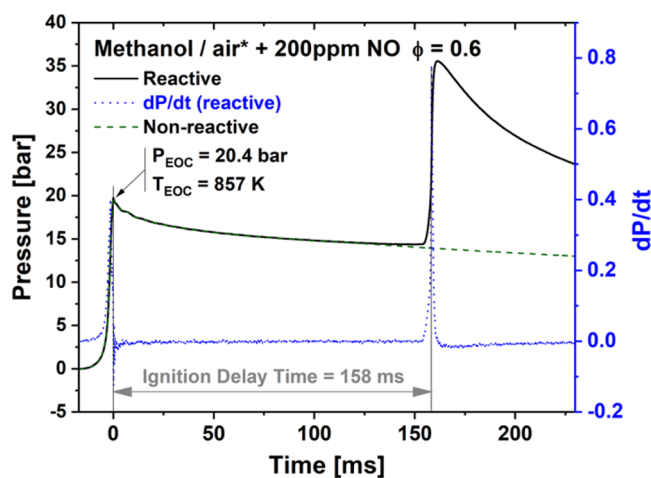

Figure 1. Representative pressure profile of the KAUST RCM.

chamber pressure signal was recorded using a flush-mounted Kistler 6045B pressure transducer and through a Kistler 5018 charge amplifier connected to a computer through the National Instruments DAQ system. A total of 500 ms was recorded with a 1 MHz frequency. The experimental uncertainties were estimated to be within ±20%.

2.2. Kinetic Modeling. The skeletal CH_3OH/NO_x model proposed here was constructed based on the skeletal methanol model from Pichler et al.[21] with a selected subset of NO_x and CH_3OH/NO_x reactions from a comprehensive nitrogen combustion chemistry developed by Glarborg et al.[22] The base skeletal CH_3OH (ACR55) model from Pichler et al.[21] was initially reduced from the AramcoMech 2.0 mechanism by Li et al.[23] The ACR55[21] model was validated against a selected set of ignition delay times, laminar burning velocities, and speciation profiles in methanol oxidation under the stoichiometric condition at relevant engine operating conditions (pressures of 10–50 bar and temperatures of 800–1650 K). However, in real engine combustion, a wider range of conditions are encountered, which necessitates the development of a more applicable kinetic model. Therefore, based on the ACR55[21] model, we introduced an additional reaction of HCO+H⇌CO+H_2 and modified the reaction of CH_2OH with O_2 (R1) by increasing the A-factor by a factor of 10. R1 is important in laminar flame speed predictions. This reaction rate constant has large uncertainties, which can reach as large as 10 times as reported by different studies[24−27] at high temperatures. In this work, we incorporated this adjustment into the skeletal model to improve the accuracy of methanol-premixed flame speed prediction, particularly under stoichiometric and rich conditions. Additionally, we slightly decreased the reaction rate of R2 by dividing the A-factor by 1.5 to achieve improved agreement in CH_3OH and CH_3OH/NO_x ignition performance.

$$CH_2OH + O_2 \Rightarrow CH_2O + HO_2 \tag{R1}$$

$$CH_3OH + HO_2 \Rightarrow CH_2OH + H_2O_2 \tag{R2}$$
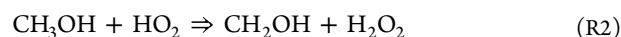
The newly added NO_x subset comprises NO_x (mainly NO and NO_2) formation reactions and CH_3OH/NO_x interactions. The thermal NO formation was adopted from Heywood et al.[28] NO can be easily converted to NO_2 via R3, converting HO_2 to the OH radical. NO_2 can also react with the H atom to recycle back to NO through R10 while releasing the OH

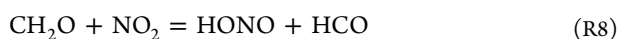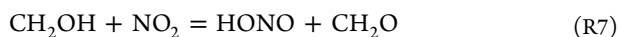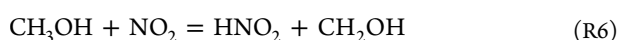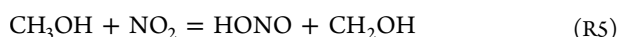**Table 1. Key Reaction Modifications in This Work[a]**

reaction	A	β	E
$CH_2OH + O_2 \Rightarrow CH_2O + HO_2$	1.6211×10^{15}	0	5017
$CH_3OH + HO_2 \Rightarrow CH_2OH + H_2O_2$	2.46×10^{13}	0	18,782
$HCO + H = CO + H2$	1.2×10^{14}	0	0
$NO + HO_2 = NO_2 + OH$	4.2×10^{11}	0	−497
$NO + OH(+M) = HONO(+M)$	2.75×10^{13}	−0.3	0
$CH_3OH + NO_2 = HONO + CH_2OH$	3×10^1	3.32	20,035
$CH_3OH + NO_2 = HNO_2 + CH_2OH$	6×10^2	2.9	27,470
$CH_2O + NO_2 = HONO + HCO$	7×10^{-8}	5.64	9220

[a]Parameters for use in the modified Arrhenius expression $k = AT\beta \exp(−E/[RT])$. Units are mol, cm, s, cal.

Table 2. Literature and New Experiments of CH_3OH and CH_3OH/NO_x Combustion under Engine Combustion Conditions

mixture	experiments	P (bar)	T (K)	equivalence ratio	additives	ref
CH_3OH	LBV	1 atm	343 K	0.7−1.5	-	32−34
			298−358 K			
			500−600 K			
		1−10 atm	423 K			24
	ST	20−50 atm	950−1250 K	0.5−2		35
	(supercritical pressure) SP-JSR	10, 100 atm	550−950 K	0.1−9		36
CH_3OH/NO_x	RCM	20−30 bar	850−950 K	0.6−1	200 ppmv NO	current
					200 ppmv NO_2	
	JSR	10 atm	700−1100 K	1	250 ppmv NO	17
					30 ppmv NO_2	

radical. With the presence of NO/NO_2 in the mixture pool, the NO/NO_2 species can react with methanol and intermediate species. These reactions could play an important role in the global combustion reactivity at low and intermediate temperatures.[29,30] To properly account for the NO/NO_2 effect on methanol combustion, a selected set of interaction reactions between NO/NO_2 with a CH_3OH subset were adopted from Glarbrog et al.[22] New nitrogen-containing species, such as HONO, HNO, and HNO_2, were introduced with corresponding reactions. HONO, as one of the key species, is formed through H-abstraction reactions involving NO_2 by either the HO_2 radical (R4) or CH_3OH (R5), CH_2OH (R7), and CH_2O species (R8). Additionally, HONO can undergo thermal decomposition, generating NO and OH radicals (R9).

$$NO + HO_2 = NO_2 + OH \qquad (R3)$$

$$NO_2 + HO_2 = HONO + O_2 \qquad (R4)$$

$$CH_3OH + NO_2 = HONO + CH_2OH \qquad (R5)$$

$$CH_3OH + NO_2 = HNO_2 + CH_2OH \qquad (R6)$$

$$CH_2OH + NO_2 = HONO + CH_2O \qquad (R7)$$

$$CH_2O + NO_2 = HONO + HCO \qquad (R8)$$

$$HONO + (M) = NO + OH(+M) \qquad (R9)$$

$$NO_2 + H = NO + OH \qquad (R10)$$

To improve the agreement with newly measured RCM experiments for CH_3OH/NO_x mixtures, we modified the Arrhenius A-factors for the important cross reactions (R3, R5,R6, R8,R9) within reasonable uncertainties (2−5 times). The modified reactions in this work are summarized in Table 1. The present skeletal model overall contains 25 species and

55 irreversible and 27 reversible reactions, which is small enough for CFD simulations.

The thermodynamic and transport data for N-containing species were adopted from Lamoureux et al.[31] The thermodynamic, transport, and kinetic files of the present skeletal model are provided in the Supporting Information.

2.3. Simulation Methods. ChemKin-Pro software was employed for all simulations.[37] Simulation conditions for new and literature experiments are summarized in Table 2. RCM and shocktube (ST) experiments were simulated using a zero-dimensional (0D) closed homogeneous batch reactor. Measured compression volume profiles were added to account for heat loss effects in the RCM simulations. The maximum pressure gradient was used as the criterion for calculating the ignition delay times. The laminar burning velocities were computed with the premixed laminar flame-speed module. The simulations were converged to a grid-independent solution by assigning both GRAD and CURV values of 0.02, with multicomponent transport equations and thermal effects considered. JSR experiments were simulated by using the transient perfectly stirred reactor model. The flow residence time is determined by the ratio of reactor volume to mixture volume flow rate at experimental temperatures and pressures.

3. RESULTS AND DISCUSSION

The present skeletal CH_3OH/NO_x model was assessed against a large set of published and new experimental data of CH_3OH and CH_3OH/NO_x combustion. The validation targets include the laminar flame speed, ignition delay time, and speciation data. The base methanol (ACR55)[21] and literature-detailed CH_3OH/NO_x (Glarborg_2018)[22] models were also evaluated for comparison and discussion.

3.1. Methanol Oxidation Validations. *3.1.1. Laminar Burning Velocities.* Figure 2 compares the ACR55[21] and
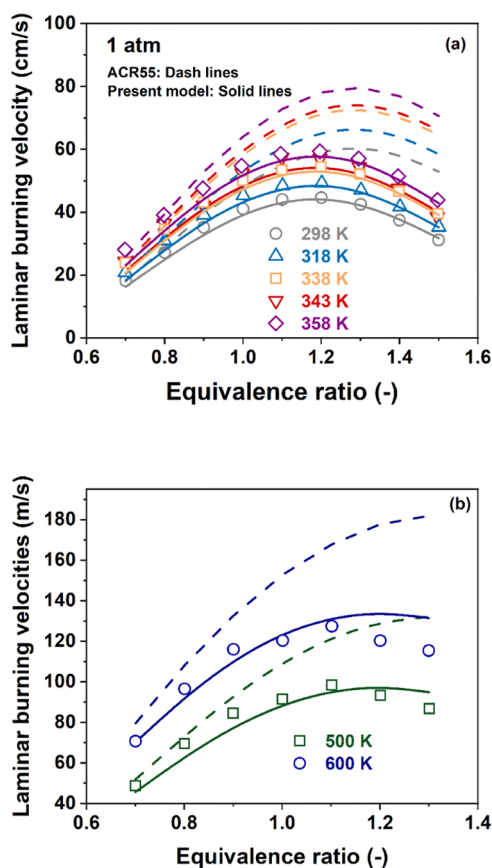
Figure 2. Measured and predicted laminar burning velocities of CH_3OH/air at various initial temperatures from 298 to 358 K (a) and 500−600 K (b) at 1 atm. Symbols are the experimental results adopted from refs 32−34 and lines are the simulation results by ACR55[21] (dash lines) and the present model (solid lines).
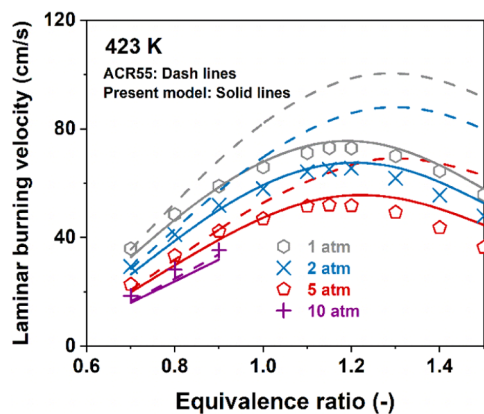

Figure 3. Measured and predicted laminar burning velocities of CH_3OH/air at the initial temperature of 423 K and pressures from 1 to 10 atm. Symbols are the experimental results adopted from ref 24 and lines are the simulation results predicted by ACR55[21] (dash lines) and the present model (solid lines).

Figure 4. Measured and predicted ignition delay times of methanol at high temperatures from 950 to 1250 K and pressures from 20 to 50 atm at (a) Φ = 0.5, (b) Φ = 1, and (c) Φ = 2. Symbols are the experimental data adopted from ref 35 and lines are simulation results by ACR55[21] (dash lines) and the present model (solid lines).

present model simulation results with literature experimental measurements[32−34] of methanol laminar burning velocities at various initial temperatures at atmospheric pressure. The ACR55 model[21] exhibits good agreement with experimental data at initial temperatures of 298−358 K under lean conditions. However, it significantly overestimates the laminar burning velocities against experiments under stoichiometric to
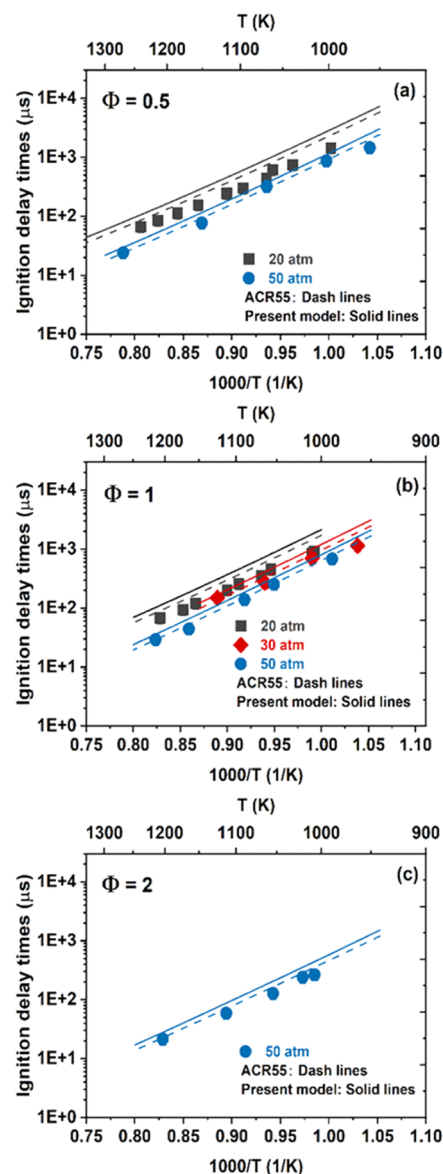
rich conditions. Moreover, it is noted that at a higher initial temperature of 600 K, as shown in Figure 2b, the ACR55 model slightly predicts higher laminar flame velocities in lean conditions while largely overpredicts laminar flame velocities in rich conditions. In contrast, the present model achieves good agreement with experimental data across a wide range of equivalence ratios and initial temperatures. We also compared the ACR55 model[21] and the present model simulation results with experimental data[24] at an elevated initial temperature of 423 K and pressures from 1 to 10 atm, as shown in Figure 3. The results demonstrate that the present skeletal model can effectively reproduce the laminar burning velocities of methanol/air mixtures at high temperatures and various pressures over a wide range of equivalence ratios. Nevertheless, the ACR55 model[21] still overestimates the laminar burning velocities under stoichiometric and rich conditions.
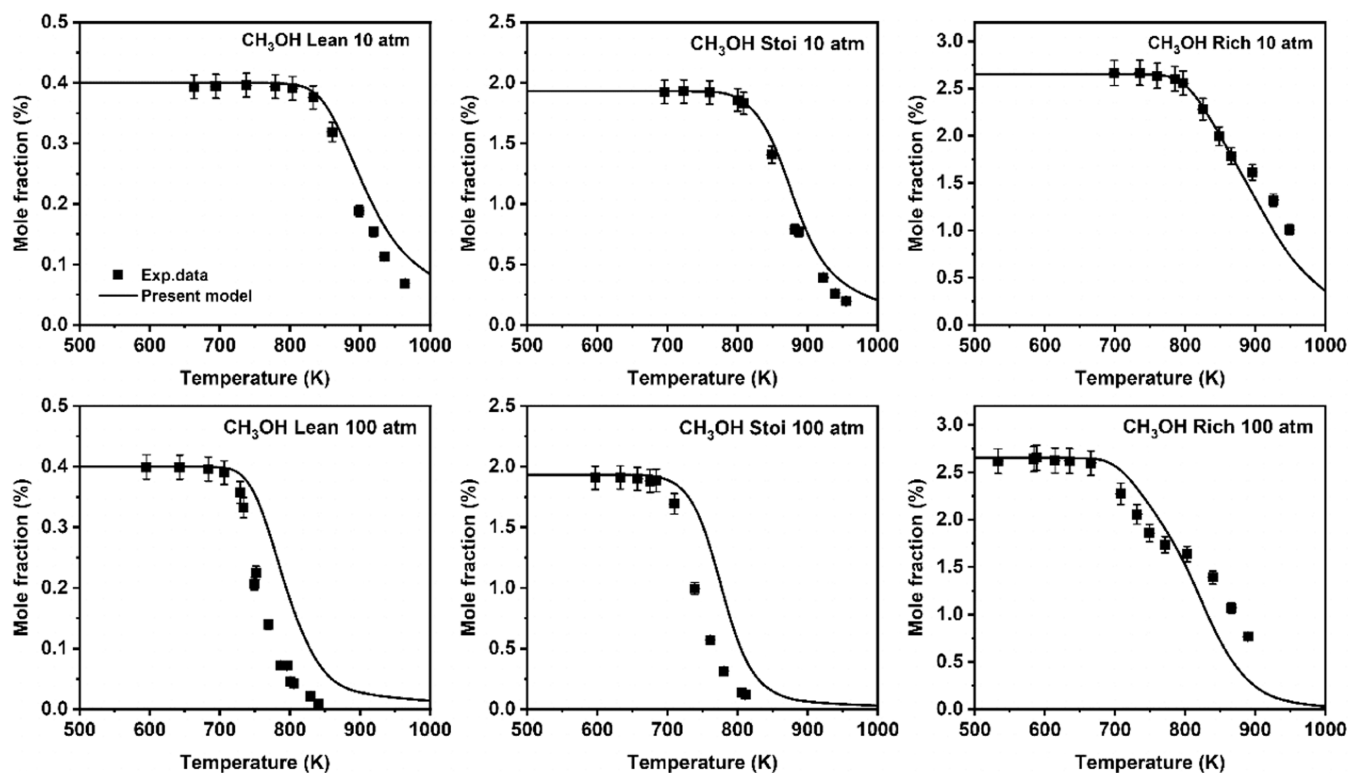
Figure 5. Measured and predicted profile of methanol oxidation at high pressures from 10 to 100 atm over a wide range of temperatures from 550 to 950 K at various equivalence ratios (lean: $\Phi = 0.1$; stoi: $\Phi = 1$; rich: $\Phi = 9$). Symbols are the experimental data adopted from ref 36 and lines are simulation results by the present model (solid lines).

3.1.2. Ignition Delay Times. The ignition delay time is also a crucial parameter for predicting combustion behavior, which is essential for model validations. Figure 4 compares the ACR55[21] and present skeletal model simulation results with literature shock tube[35] measured ignition delay times of methanol/air mixtures at high temperatures from 950 to 1250 K and high pressures of 20−50 atm over a wide range of equivalence ratios ($\Phi = 0.5$−2). The results demonstrate that the present skeletal model exhibits a slightly lower reactivity than the ACR55 model. While the present model slightly overestimates the ignition delay times against experiments at 20 atm, it performs better at a higher pressure of 50 atm. In general, the present model yields a comparable performance with the ACR55[21] model and maintains good agreement with measured ignition delay times over a wide range of equivalence ratios at high temperatures and pressures.

3.1.3. Methanol Profile at High Pressures. Besides laminar burning velocities and ignition delay times, this work further assessed the model performance at elevated high pressures against recent SP-JSR experiments.[36] Figure 5 depicts the evolution of the CH_3OH mole fraction at high pressures of 10 and 100 atm, encompassing temperatures ranging from 550 to 950 K. The present model exhibits good agreement with measured methanol profiles at 10 atm across a wide range of operating conditions. However, at an elevated pressure of 100 atm, the model underpredicts the methanol consumption in the temperature range of 750−850 K in ultralean ($\Phi = 0.1$) and stoichiometric ($\Phi = 1$) conditions. Despite this, the model demonstrates the ability to capture the methanol consumption behavior reasonably well under high pressures and various operating conditions, which underscores its practical applicability in real engine combustion systems.

3.2. NO$_x$ Impact on Methanol Oxidation. *3.2.1. New RCM Experiments of $CH_3OH/NO/NO_2$.* NO/NO_2 has been found to exhibit strong effects on fuel ignition under high-pressure conditions.[38−40] However, the impact of NO/NO_2 addition on the ignition performance of methanol is still scarcely investigated due to a lack of experimental studies. To address this gap, new RCM experiments were conducted to investigate the ignition performance of $CH_3OH/NO/NO_2$ mixtures under lean ($\Phi = 0.6$) and stoichiometric ($\Phi = 1$) conditions at engine operating-relevant conditions (20−30 bar, 850−950 K). Figure 6 compares the newly measured ignition delay times of $CH_3OH/NO/NO_2$ mixtures and simulation results predicted by the present model under different operating conditions.

From new experiments, results indicate that the presence of 200 ppmv NO or NO_2 leads to an increase in mixture reactivity for both lean and stoichiometric conditions, thus enhancing the autoignition performance of methanol. However, it is observed that these reactivity-enhancing effects diminish as temperature increases. Additionally, NO_2 exhibits a slightly more pronounced promotion effect on methanol autoignition compared to that of NO, despite the same concentration added. Similar observations were found under the stoichiometric conditions, as illustrated in Figure 6b. Moreover, the addition of NO/NO_2 consistently enhances the ignition performance of methanol under varying pressures of 20 and 30 bar. These findings emphasize the importance of the $CH_3OH/NO/NO_2$ interactions in the fuel ignition process.

Upon comparison of the simulation results with experimental data, the present skeletal model exhibits an overall good agreement against new experiments, which effectively reproduces the effects of NO/NO_2 additions on methanol
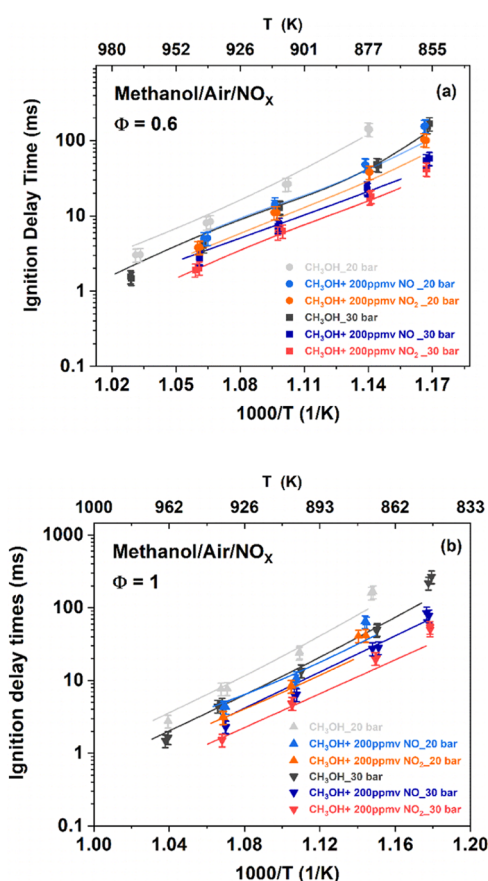
Figure 6. Comparison of the present skeletal model (solid lines) simulation results with newly measured RCM ignition delay times (symbols) of methanol with the addition of 200 ppmv of NO/NO_2 at $\Phi = 0.6$ (a) and $\Phi = 1$ (b) at 20 and 30 bar.

Figure 7. Comparison of the detailed Glarborg_2018 model[22] (short dash lines) and the present skeletal model (solid lines) simulation results with newly measured RCM ignition delay times (symbols) of methanol with the addition of 200 ppmv NO/NO_2 at $\Phi = 0.6$ (a) and $\Phi = 1$ (b) at 30 bar.

autoignition. However, some discrepancies were noted in the compressed temperature predictions, especially in the presence of NO/NO_2. Specifically, in the lean condition, the skeletal model accurately predicts the compressed temperatures in neat methanol ignition case. However, with the introduction of NO/NO_2 at 30 bar, the model overestimates the compressed temperatures. Similarly, under the stoichiometric conditions, this model slightly predicts higher compressed temperatures in the presence of NO_2 at 20 bar. These discrepancies can be attributed to both modeling and experimental aspects. The experimental measurement uncertainties were within 5 K, possibly due to reactivity change with the presence of oxygen in reactive mixtures during the compression phase. On the modeling side, the unpredicted compressed temperature may arise from the increased reactivity in the presence of NO_x during the compression phase.

Figure 7 compares simulation results predicted by the present skeletal model and the detailed model from Glarborg et al.[22] against experiments at 30 bar. In a previous study,[41] the performance of the Glarborg_2018[22] model was assessed in simulating CH_3OH/NO_x and formaldehyde $(CH_2O)/NO_x$ interactions against a large number of existing experiments, covering a wide range of conditions. This study[41] revealed that among various detailed reaction mechanisms, the Glarborg_2018[22] model exhibited the best accuracy in reproducing these experiments. However, in the current study, when the Glarborg_2018[22] model is evaluated against new experiments, it is observed that the detailed model fails to accurately predict
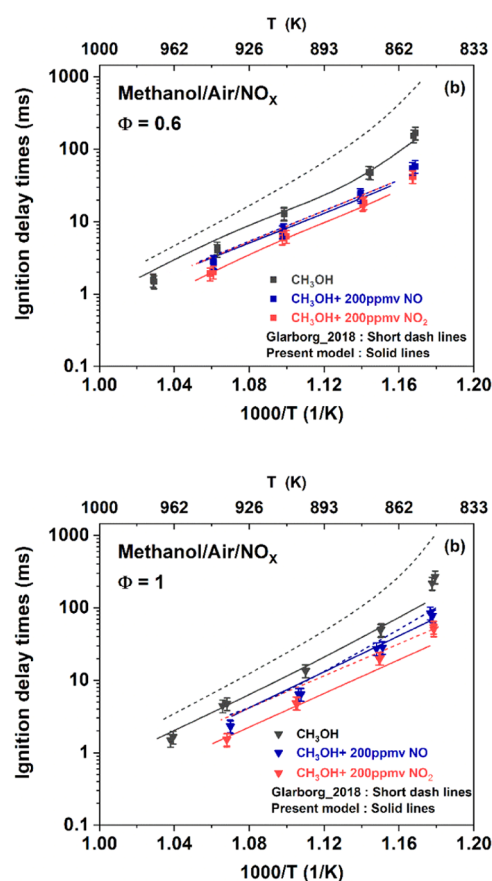
the ignition delay times of pure methanol. Furthermore, the detailed model predicts similar ignition delay times for methanol in the presence of 200 ppmv NO or 200 ppmv NO_2. Additionally, it should be noted that the detailed model predicts similar compressed temperatures as the present model. Discrepancies are also observed in the compressed temperature predictions under lean conditions, where the detailed model predicts higher compressed temperatures in comparison to the experimental measurements. Overall, the present skeletal model exhibits improved performance when compared to the detailed model.

To better understand the performance of the skeletal model in RCM conditions, the major NO_x reaction pathways are analyzed at 850 K, 30 bar, $\Phi = 0.6$, and around 1.3% fuel consumption using the present model, as depicted in Figure 8. Our analyses reveal that H-abstraction reactions from CH_3OH by OH and HO_2 play a pivotal role in the initial steps of methanol oxidation, both in the absence and presence of NO_x species. However, in the presence of NO/NO_2, it can be noted that the H-abstraction from CH_3OH by the HO_2 radical is decreased, while the H-abstraction from CH_3OH by the OH radical becomes more pronounced. In addition, a new reaction pathway of R5 is identified to participate in the initiation of CH_3OH oxidation in the presence of NO_x species. For the subsequent reactions, it is also noted that CH_2O+OH is increased, while CH_2O+HO_2 is slightly decreased with the presence of NO_x.
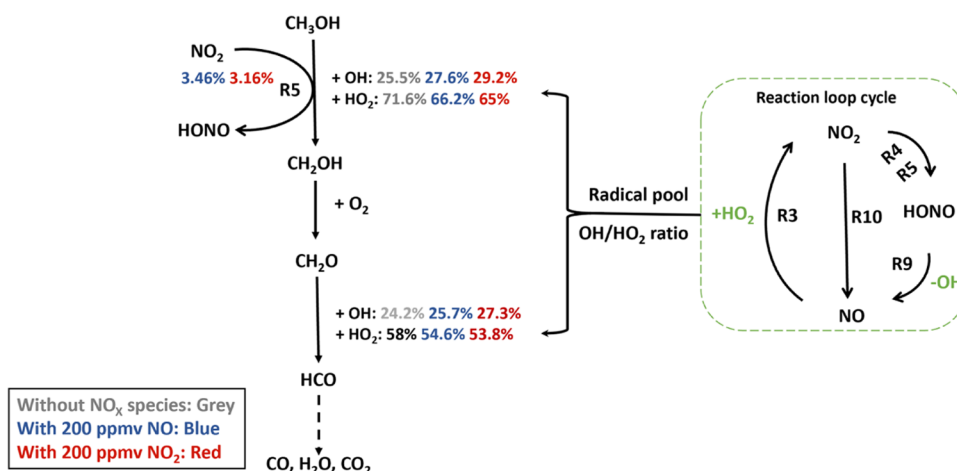
Figure 8. Major reaction pathway analyses for methanol consumption without and with the presence of 200 ppmv NO/NO$_2$ at a compression pressure of 30 bar, compression temperature of 850 K, Φ = 0.6, and around 1.3% methanol consumption using the present model.
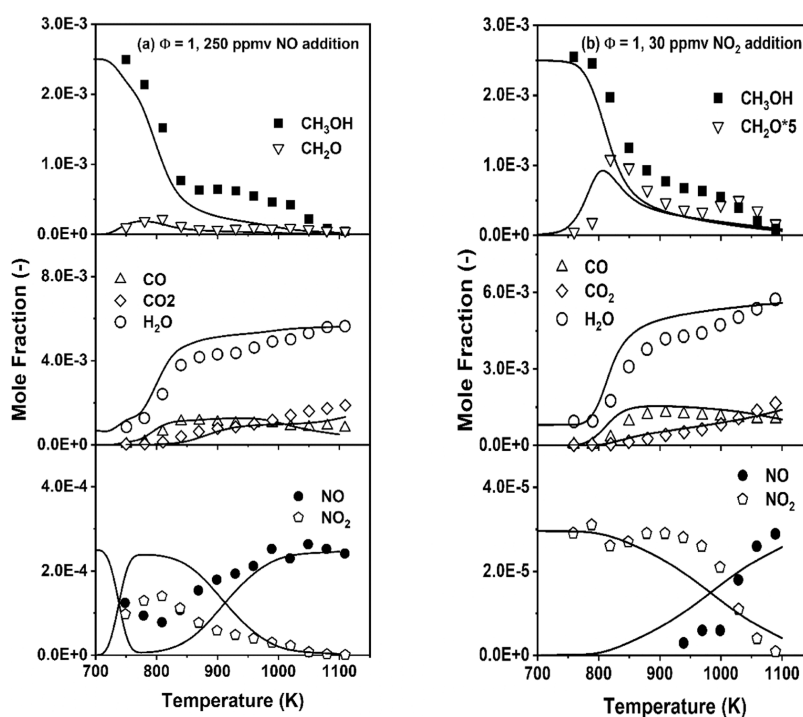

Figure 9. Comparison between the skeletal model simulation results (solid lines) with measured species profiles (symbols) of methanol oxidation with the presence of 250 ppmv NO (a) and 30 ppmv NO$_2$ (b) at Φ = 1 and 10 atm. Symbols are the experimental data adopted from ref 17 and lines are simulation results by the present model (solid lines).

To further understand differences in NO/NO$_2$ effects on methanol ignition, a reaction loop cycle involving NO, NO$_2$, and HONO is presented in Figure 8. In the presence of NO, NO is initially converted to NO$_2$ through R3. Subsequently, a portion of NO$_2$ can undergo further reaction with CH$_3$OH, forming HONO via R5. Furthermore, NO$_2$ undergoes conversion back to NO via R9, while HONO decomposes (R10), yielding NO and releasing OH radicals. In the presence of NO$_2$, NO$_2$ primarily reacts with HO$_2$ or CH$_3$OH, leading to the initial formation of HONO via R4 and R5. Similar to the previously mentioned pathways (R9 and R10), NO$_2$ undergoes recycling back to NO, and the decomposition of HONO generates NO and OH radicals. This reaction cycle involving NO → NO$_2$ → HONO → NO converts the less reactive HO$_2$ radical to the OH radical, profoundly enhancing the reactivity

of the fuel mixture system. Consequently, this contributes to increased H-abstraction reactions of CH$_3$OH by OH radicals.

In summary, NO$_x$ species mainly play a catalytic role by going through a reaction loop cycle in the oxidation of methanol, resulting in the formation of more OH radicals that promote fuel oxidation initiation and chain branching reactions. Besides the catalytic effect, NO$_2$ could actively participate in the direct methanol oxidation process.

3.2.2. Literature JSR Experiments of CH$_3$OH/NO/NO$_2$. In addition to the ignition delay time validations, the skeletal model was also evaluated in literature JSR experiments[17] of methanol oxidation with the presence of 250 ppmv NO and 30 ppmv NO$_2$, respectively, under the stoichiometric condition at 10 atm. The comparison between simulation results and measured major species profiles is illustrated in Figure 9. The
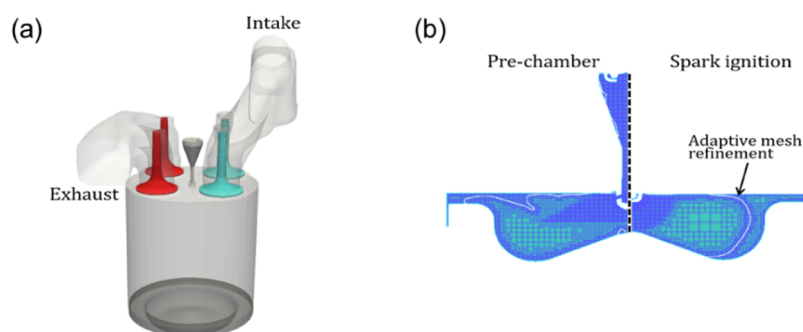
Figure 10. (a) Fluid domain and (b) mesh details during combustion.

present skeletal model captures the overall trends for fuel consumption and pollutant formation (CO, CO_2, and CH_2O) quite well. However, it is observed that the current skeletal model tends to overpredict the conversion of NO to NO_2 during methanol oxidation in the presence of NO while simultaneously underpredicting the conversion of NO_2 to NO in methanol oxidation with the presence of NO_2. These discrepancies are linked to NO to NO_2 conversion reactions, such as $NO + HO_2 = NO_2 + OH$. It is worth noting that this reaction also plays a crucial role in predicting ignition delay times due to OH radical production. Overall, the predicted qualitative trends for the NO to NO_2 conversion align closely with the observed experimental trends.

4. MODEL ASSESSMENT USING CFD

To assess the newly developed kinetic mechanism under engine conditions, CFD simulations were performed by using

Table 3. Engine Details and Operating Conditions

engine model	Volvo D13C500
piston shape	bowl-in-piston
valve mechanism	single overhead cam
number of valves	2-intake 2-exhaust
bore	131 mm
stroke	158 mm
connecting rod length	265 mm
compression ratio	11.5
displacement volume	2.1 L
engine speed	1200 rpm
air-fuel ratio (λ)	1.4 and 1.6

Table 4. Engine Operating Conditions

	case 1	case 2	case 3
engine configuration	SI	SI	PC
spark timing [CAD aTDC]	−29	−40	−15
air−fuel ratio − λ	1.4	1.6	1.6
intake pressure (bar)	1.0	1.0	1.0

CONVERGE. Following the increasing efforts toward lean burn engines, the available in-house experimental data was leveraged to verify the chemical model fidelity under practically relevant conditions. Two configurations were tested: spark ignition (SI) and passive prechamber (PC). Details on extensive modeling settings for both engines are shown in previous works.[42−44] The computational geometry and mesh structures are shown in Figure 10. For the SI operation, the prechamber hardware is simply replaced by a spark plug.

Details of engine configurations and prechamber specifications are found in other studies.[45,46] The schematic of the testbed is found in refs 45−47. Fuel injectors are installed in the air intake ports. Tables 3 and 4 include details about the engine and its operating parameters, respectively.

The turbulent transport equations were solved using the Reynolds-averaged Navier−Stokes (RANS) formulation with the RNG k-ε model.[48] For combustion closure, the multizone well-stirred reactor[49] was adopted. The spark energy deposition was considered as a spherical source placed in the spark plug gap, delivering 0.06 J in total. The PISO algorithm[50] was used to couple pressure and velocity. The wall heat transfer was accounted for with the O'Rourke and Amsden[51] model. Further details on computational setup can be found in other works.[52] The model was initialized quiescently at the exhaust valve opening (EVO); a full-cycle simulation was performed aiming to minimize any error influence in the pressure, velocity, and composition field initialization. The intake inflow boundary was considered homogeneous with the air−fuel ratio (λ) shown in Table 4.

The results for the mean pressure with the 500 cycles (gray) and key engine performance metrics are shown in Figure 11a−c, respectively. Good agreement with the experimental measurements was obtained, thus demonstrating the capability of the chemical kinetic model for engine-relevant conditions. Minor differences commonly arise from modeling/experimental approximations, such as blow-by, crankshaft deflection, and homogeneous intake charge assumption. Nonetheless, the trends of practical interest were well captured. While discussions on engine optimization and best operating conditions are reported in previous works,[53] the current validation suffices to demonstrate the capability of the model at multiple conditions. More critically, lean engine operation covers a vast portion of the current engineering focus, and the current model well serves the desired purpose with sufficient success. While most of the improvements in the new chemical mechanism reside in the stoichiometric and rich regions, future verification will be performed once in-house data under those conditions are available.

5. CONCLUSIONS

In conclusion, this study developed and validated a skeletal CH_3OH/NO_x kinetic model for full-cycle simulations of engine combustion by using methanol. The new RCM experiments under engine-relevant conditions demonstrate notable enhancement effects of NO/NO_2 additions on methanol ignition. The inclusion of the CH_3OH/NO_x interaction in the kinetic model was then identified to be important for accurately predicting methanol combustion
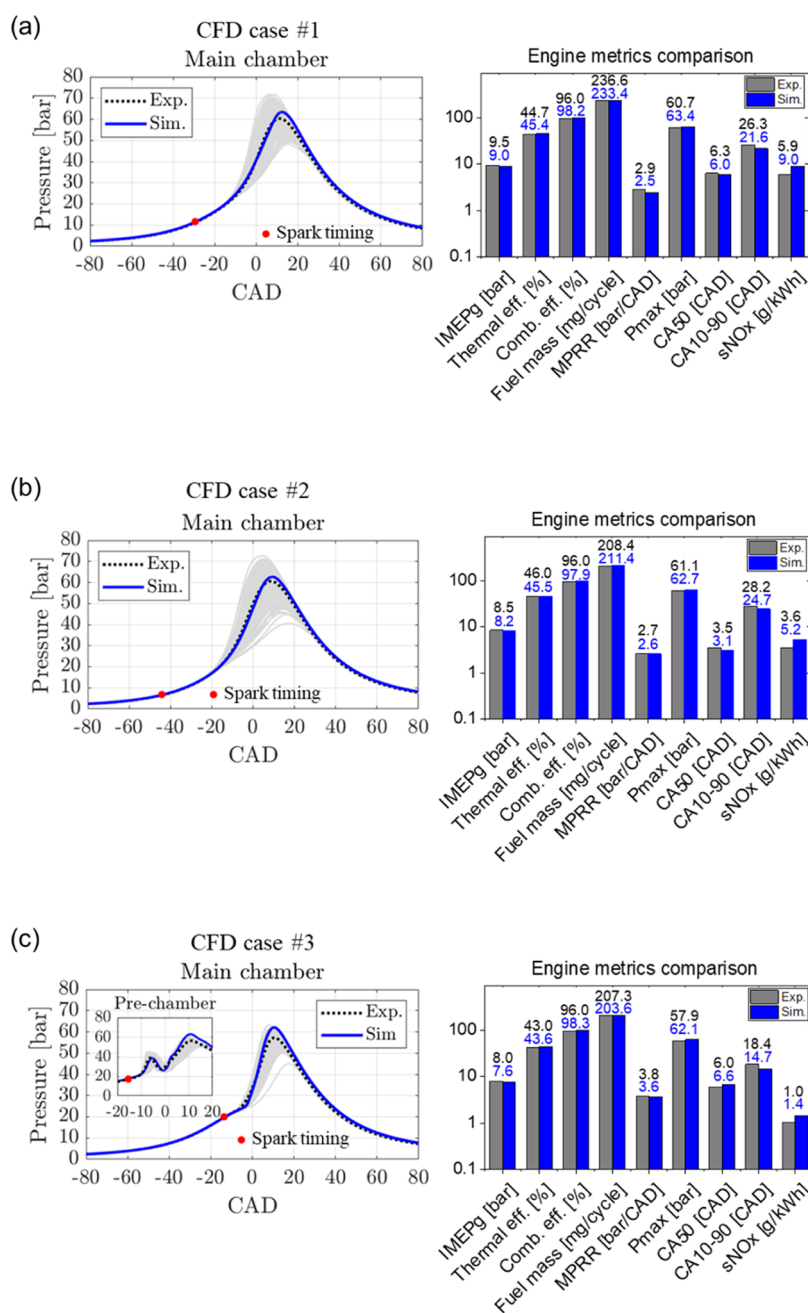
Figure 11. Pressure and engine metrics comparison between experiments and simulations for (a) case 1: SI engine at $\lambda = 1.4$, (b) case 2: SI engine at $\lambda = 1.6$, and (c) case 3: PC engine at $\lambda = 1.6$.

performance considering the residual gas recirculation. The proposed skeletal mechanism, consisting of 25 species, 55 irreversible reactions, and 27 reversible reactions, was validated against literature data and new methanol/methanol–NO_x experiments across a wide range of operating conditions. This confirms the reliability and applicability of the skeletal model for predicting methanol combustion behavior in engine combustion systems. Furthermore, the skeletal mechanism was employed in 3D CFD simulations of engine combustion using methanol. The simulation results exhibit good agreement with experimental measurements of pressure traces and engine metrics, indicating that the proposed model is suitable and sufficient for CFD simulations. Overall, this work contributes to the advancement of understanding methanol combustion and its interaction with NO/NO_2 in engine applications. The

developed skeletal CH_3OH/NO_x kinetic model provides valuable insight for CFD modeling studies aimed at optimizing engine performance, achieving better combustion efficiency, and reducing exhaust emissions when utilizing methanol as a renewable fuel.

■ ASSOCIATED CONTENT

ⓈI Supporting Information

The Supporting Information is available free of charge at https://pubs.acs.org/doi/10.1021/acsomega.3c06488.

RCM experimental data and the developed skeletal CH3OH/NO_x kinetic model, including thermodynamic, transport, and kinetic files (ZIP)

■ AUTHOR INFORMATION

Corresponding Author

    Wenxian Tang − *King Abdullah University of Science and Technology, Thuwal 23955, Saudi Arabia;* ⊙ orcid.org/0009-0007-1409-6778; Email: wenxian.tang@kaust.edu.sa

Authors

    Mickael Silva − *King Abdullah University of Science and Technology, Thuwal 23955, Saudi Arabia*

    Khaiyom Hakimov − *King Abdullah University of Science and Technology, Thuwal 23955, Saudi Arabia*

    Xiaoyuan Zhang − *King Abdullah University of Science and Technology, Thuwal 23955, Saudi Arabia; Department of Thermal Science and Energy Engineering, University of Science and Technology of China (USTC), Hefei, Anhui 230026, China;* ⊙ orcid.org/0000-0003-3043-1859

    Ponnya Hlaing − *King Abdullah University of Science and Technology, Thuwal 23955, Saudi Arabia;* ⊙ orcid.org/0000-0003-2007-0121

    Emre Cenker − *Saudi Aramco Research and Development Center, Transport Technologies Division Dhahran, Eastern 31311, Saudi Arabia*

    Abdullah S. AlRamadan − *Saudi Aramco Research and Development Center, Transport Technologies Division Dhahran, Eastern 31311, Saudi Arabia*

    James W. G. Turner − *King Abdullah University of Science and Technology, Thuwal 23955, Saudi Arabia*

    Aamir Farooq − *King Abdullah University of Science and Technology, Thuwal 23955, Saudi Arabia;* ⊙ orcid.org/0000-0001-5296-2197

    Hong G. Im − *King Abdullah University of Science and Technology, Thuwal 23955, Saudi Arabia*

    S. Mani Sarathy − *King Abdullah University of Science and Technology, Thuwal 23955, Saudi Arabia;* ⊙ orcid.org/0000-0002-3975-6206

Complete contact information is available at:
https://pubs.acs.org/10.1021/acsomega.3c06488

Notes

The authors declare no competing financial interest.

■ REFERENCES

(1) Xing, H.; Stuart, C.; Spence, S.; Chen, H. Alternative Fuel Options for Low Carbon Maritime Transportation: Pathways to 2050. *J. Cleaner Prod.* **2021**, *297*, No. 126651.

(2) Harris, K.; Grim, R. G.; Huang, Z.; Tao, L. A Comparative Techno-Economic Analysis of Renewable Methanol Synthesis from Biomass and CO2: Opportunities and Barriers to Commercialization. *Appl. Energy* **2021**, *303*, No. 117637.

(3) Zhen, X.; Wang, Y.; Xu, S.; Zhu, Y. Study of Knock in a High Compression Ratio Spark-Ignition Methanol Engine by Multi-Dimensional Simulation. *Energy* **2013**, *50*, 150−159.

(4) Nichols, R. J. The Methanol Story: A Sustainable Fuel for the Future. *J. Sci. Ind. Res.* **2003**, *62*, 97−105.

(5) Zhen, X.; Wang, Y. An Overview of Methanol as an Internal Combustion Engine Fuel. *Renewable Sustainable Energy Rev.* **2015**, *52*, 477−493.

(6) Abd-Alla, G. H. Using Exhaust Gas Recirculation in Internal Combustion Engines: A Review. *Energy Convers. Manage.* **2002**, *43* (8), 1027−1042.

(7) Agarwal, D.; Singh, S. K.; Agarwal, A. K. Effect of Exhaust Gas Recirculation (EGR) on Performance, Emissions, Deposits and Durability of a Constant Speed Compression Ignition Engine. *Appl. Energy* **2011**, *88* (8), 2900−2907.

(8) Haskara, I.; Zhu, G. G.; Winkelman, J. In *Multivariable EGR/Spark Timing Control for IC Engines via Extremum Seeking*, 2006 American Control Conference, IEEE, 2006; p 6.

(9) Li, W.; Liu, Z.; Wang, Z.; Xu, Y. Experimental Investigation of the Thermal and Diluent Effects of EGR Components on Combustion and NOx Emissions of a Turbocharged Natural Gas SI Engine. *Energy Convers. Manage.* **2014**, *88*, 1041−1050.

(10) Vancoillie, J.; Christensen, M.; Nilsson, E. J. K.; Verhelst, S.; Konnov, A. A. The Effects of Dilution with Nitrogen and Steam on the Laminar Burning Velocity of Methanol at Room and Elevated Temperatures. *Fuel* **2013**, *105*, 732−738.

(11) Koda, S.; Tanaka, M. Ignition of Premixed Methanol/Air in a Heated Flow Tube and the Effect of NO2 Addition. *Combust. Sci. Technol.* **1986**, *47* (3−4), 165−176.

(12) Hirano, M.; Oda, K.; Hirano, T.; Akita, K. Burning Velocities of Methanol-Air-Water Gaseous Mixtures. *Combust. Flame* **1981**, *40*, 341−343.

(13) Hjuler, K.; Glarborg, P.; Dam-Johansen, K. Mutually Promoted Thermal Oxidation of Nitric Oxide and Organic Compounds. *Ind. Eng. Chem. Res.* **1995**, *34* (5), 1882−1888.

(14) Lyon, R. K.; Cole, J. A.; Kramlich, J. C.; Chen, S. L. The Selective Reduction of SO3 to SO2 and the Oxidation of NO to NO2 by Methanol. *Combust. Flame* **1990**, *81* (1), 30−39.

(15) Alzueta, M. U.; Røjel, H.; Kristensen, P. G.; Glarborg, P.; Dam-Johansen, K. Laboratory Study of the CO/NH3/NO/O2 System: Implications for Hybrid Reburn/SNCR Strategies. *Energy Fuels* **1997**, *11* (3), 716−723.

(16) Moréac, G.; Dagaut, P.; Roesler, J. F.; Cathonnet, M. Nitric Oxide Interactions with Hydrocarbon Oxidation in a Jet-Stirred Reactor at 10 Atm. *Combust. Flame* **2006**, *145* (3), 512−520.

(17) Dayma, G.; Ali, K. H.; Dagaut, P. Experimental and Detailed Kinetic Modeling Study of the High Pressure Oxidation of Methanol Sensitized by Nitric Oxide and Nitrogen Dioxide. *Proc. Combust. Inst.* **2007**, *31* (1), 411−418.

(18) Hakimov, K.; Arafin, F.; Aljohani, K.; Djebbi, K.; Ninnemann, E.; Vasu, S. S.; Farooq, A. Ignition Delay Time and Speciation of Dibutyl Ether at High Pressures. *Combust. Flame* **2021**, *223*, 98−109.

(19) Issayev, G. Autoignition and Reactivity Studies of Renewable Fuels and Their Blends with Conventional Fuels. Doctoral Dissertation, 2021.

(20) Le, M. D.; Matrat, M.; Amara, A. B.; Foucher, F.; Moreau, B.; Yu, Y.; Glaude, P.-A. Chemical Effects of Ferrocene and 2-Ethylhexyl Nitrate on a Low-Octane Gasoline: An Experimental and Numerical RCM Study. *Proc. Combust. Inst.* **2021**, *38* (1), 441−448.

(21) Pichler, C.; Nilsson, E. J. K. Reduced Kinetic Mechanism for Methanol Combustion in Spark-Ignition Engines. *Energy Fuels* **2018**, *32* (12), 12805−12813.

(22) Glarborg, P.; Miller, J. A.; Ruscic, B.; Klippenstein, S. J. Modeling Nitrogen Chemistry in Combustion. *Prog. Energy Combust. Sci.* **2018**, *67*, 31−68.

(23) Li, Y.; Zhou, C.-W.; Somers, K. P.; Zhang, K.; Curran, H. J. The Oxidation of 2-Butene: A High Pressure Ignition Delay, Kinetic Modeling Study and Reactivity Comparison with Isobutene and 1-Butene. *Proc. Combust. Inst.* **2017**, *36* (1), 403−411.

(24) Zhang, X.; Wang, G.; Zou, J.; Li, Y.; Li, W.; Li, T.; Jin, H.; Zhou, Z.; Lee, Y.-Y. Investigation on the Oxidation Chemistry of

Methanol in Laminar Premixed Flames. *Combust. Flame* **2017**, *180*, 20−31.

(25) Christensen, M.; Nilsson, E. J. K.; Konnov, A. A. A Systematically Updated Detailed Kinetic Model for CH2O and CH3OH Combustion. *Energy Fuels* **2016**, *30* (8), 6709−6726.

(26) Dames, E. E.; Golden, D. M. Master Equation Modeling of the Unimolecular Decompositions of Hydroxymethyl (CH2OH) and Methoxy (CH3O) Radicals to Formaldehyde (CH2O) + H. *J. Phys. Chem. A* **2013**, *117* (33), 7686−7696.

(27) Hippler, H.; Striebel, F.; Viskolcz, B. A Detailed Experimental and Theoretical Study on the Decomposition of Methoxy Radicals. *Phys. Chem. Chem. Phys.* **2001**, *3* (12), 2450−2458.

(28) *Internal Combustion Engine Fundamentals*, 2nd ed..; Heywood, J. B., Ed.; McGraw-Hill Education, 2018.

(29) Combustion Chemistry of Ammonia/C1 Fuels: A Comprehensive Kinetic Modeling Study, 2023. https://www.sciencedirect.com/science/article/pii/S0016236123002892.

(30) Li, M.; He, X.; Hashemi, H.; Glarborg, P.; Lowe, V. M.; Marshall, P.; Fernandes, R.; Shu, B. An Experimental and Modeling Study on Auto-Ignition Kinetics of Ammonia/Methanol Mixtures at Intermediate Temperature and High Pressure. *Combust. Flame* **2022**, *242*, No. 112160.

(31) Lamoureux, N.; Merhubi, H. E.; Pillier, L.; de Persis, S.; Desgroux, P. Modeling of NO Formation in Low Pressure Premixed Flames. *Combust. Flame* **2016**, *163*, 557−575.

(32) Veloo, P. S.; Wang, Y. L.; Egolfopoulos, F. N.; Westbrook, C. K. A Comparative Experimental and Computational Study of Methanol, Ethanol, and n-Butanol Flames. *Combust. Flame* **2010**, *157* (10), 1989−2004.

(33) Sileghem, L.; Alekseev, V. A.; Vancoillie, J.; Nilsson, E. J. K.; Verhelst, S.; Konnov, A. A. Laminar Burning Velocities of Primary Reference Fuels and Simple Alcohols. *Fuel* **2014**, *115*, 32−40.

(34) Katoch, A.; Asad, M.; Minaev, S.; Kumar, S. Measurement of Laminar Burning Velocities of Methanol−Air Mixtures at Elevated Temperatures. *Fuel* **2016**, *182*, 57−63.

(35) Burke, S. M.; Burke, U.; McDonagh, R.; Mathieu, O.; Osorio, I.; Keesee, C.; Morones, A.; Petersen, E. L.; Wang, W.; DeVerter, T. A.; Oehlschlaeger, M. A.; Rhodes, B.; Hanson, R. K.; Davidson, D. F.; Weber, B. W.; Sung, C.-J.; Santner, J.; Ju, Y.; Haas, F. M.; Dryer, F. L.; Volkov, E. N.; Nilsson, E. J. K.; Konnov, A. A.; Alrefae, M.; Khaled, F.; Farooq, A.; Dirrenberger, P.; Glaude, P.-A.; Battin-Leclerc, F.; Curran, H. J. An Experimental and Modeling Study of Propene Oxidation. Part 2: Ignition Delay Time and Flame Speed Measurements. *Combust. Flame* **2015**, *162* (2), 296−314.

(36) Wang, Z.; Zhao, H.; Yan, C.; Lin, Y.; Lele, A. D.; Xu, W.; Rotavera, B.; Jasper, A. W.; Klippenstein, S. J.; Ju, Y. Methanol Oxidation up to 100 Atm in a Supercritical Pressure Jet-Stirred Reactor. *Proc. Combust. Inst.* **2023**, *39* (1), 445−453.

(37) Kee, R. J.; Rupley, F. M.; Meeks, E.; Miller, J. A. *CHEMKIN-III: A FORTRAN Chemical Kinetics Package for the Analysis of Gas-Phase Chemical and Plasma Kinetics*; SAND-96-8216; Sandia National Lab. (SNL-CA), Livermore, CA (United States), 1996. DOI: 10.2172/481621.

(38) Fang, R.; Saggese, C.; Wagnon, S. W.; Sahu, A. B.; Curran, H. J.; Pitz, W. J.; Sung, C.-J. Effect of Nitric Oxide and Exhaust Gases on Gasoline Surrogate Autoignition: Iso-Octane Experiments and Modeling. *Combust. Flame* **2022**, *236*, No. 111807.

(39) Shock-Induced Ignition of Methane, Ethane, and Methane/Ethane Mixtures Sensitized by NO2 | Energy & Fuels, 2023. https://pubs.acs.org/doi/full/10.1021/acs.energyfuels.7b01632.

(40) Ajrouche, H.; Nilaphai, O.; Hespel, C.; Foucher, F. Impact of Nitric Oxide on N-Heptane and n-Dodecane Autoignition in a New High-Pressure and High-Temperature Chamber. *Proc. Combust. Inst.* **2019**, *37* (3), 3319−3326.

(41) Kovács, M.; Papp, M.; Zsély, I. G.; Turányi, T. Main Sources of Uncertainty in Recent Methanol/NOx Combustion Models. *Int. J. Chem. Kinet.* **2021**, *53* (7), 884−900.

(42) Aljabri, H.; Silva, M.; Houidi, M. B.; Liu, X.; Allehaibi, M.; Almatrafi, F.; AlRamadan, A. S.; Mohan, B.; Cenker, E.; Im, H. G. Comparative Study of Spark-Ignited and Pre-Chamber Hydrogen-Fueled Engine: A Computational Approach. *Energies* **2022**, *15* (23), 8951.

(43) Silva, M.; Liu, X.; Hlaing, P.; Sanal, S.; Cenker, E.; Chang, J.; Johansson, B.; Im, H. G. Computational Assessment of Effects of Throat Diameter on Combustion and Turbulence Characteristics in a Pre-Chamber Engine. *Appl. Therm. Eng.* **2022**, *212*, No. 118595.

(44) Liu, X.; Echeverri Marquez, M.; Sanal, S.; Silva, M.; AlRamadan, A. S.; Cenker, E.; Sharma, P.; Magnotti, G.; Turner, J. W. G.; Im, H. G. Computational Assessment of the Effects of Pre-Chamber and Piston Geometries on the Combustion Characteristics of an Optical Pre-Chamber Engine. *Fuel* **2023**, *341*, No. 127659.

(45) Hlaing, P.; Silva, M.; Marquez, M. E.; Cenker, E.; Houidi, M. B.; Im, H. G.; Turner, J. W. G.; Johansson, B. Estimates of the Air-Fuel Ratio at the Time of Ignition in a Pre-Chamber Using a Narrow Throat Geometry, 2023. https://journals.sagepub.com/doi/abs/10.1177/14680874211059148.

(46) Hlaing, P.; Echeverri Marquez, M.; Cenker, E.; Im, H. G.; Johansson, B.; Turner, J. W. G. Effects of Volume and Nozzle Area in Narrow-Throat Spark-Ignited Pre-Chamber Combustion Engines. *Fuel* **2022**, *313*, No. 123029.

(47) Hlaing, P.; Echeverri Marquez, M.; Shankar, V.; Cenker, E.; Ben Houidi, M.; Johansson, B. *A Study of Lean Burn Pre-Chamber Concept in a Heavy Duty Engine*; SAE International, 2019.

(48) Han, Z.; Reitz, R. D. Turbulence Modeling of Internal Combustion Engines Using RNG κ-ε Models. *Combust. Sci. Technol.* **1995**, *106* (4−6), 267−295.

(49) Senecal, P. K.; Pomraning, E.; Richards, K. J.; Briggs, T. E.; Choi, C. Y.; McDavid, R. M.; Patterson, M. A. Multi-Dimensional Modeling of Direct-Injection Diesel Spray Liquid Length and Flame Lift-off Length Using CFD and Parallel Detailed Chemistry. *SAE Trans.* **2003**, *112*, 1331−1351.

(50) Issa, R. I.; Gosman, A. D.; Watkins, A. P. The Computation of Compressible and Incompressible Recirculating Flows by a Non-Iterative Implicit Scheme. *J. Comput. Phys.* **1986**, *62* (1), 66−82.

(51) Amsden, A. A. *A Computer Program for Chemically Reactive Flows with Sprays*; Los Alamos National Laboratory Report LA-11560-MS, 1989.

(52) Silva, M. M. A Numerical Investigation of Pre-Chamber Combustion Engines. Doctoral Dissertation, 2020.

(53) Liu, X.; Sharma, P.; Silva, M. Computational Investigation on the Combustion and Emission Characteristics of a Methanol Pre-Chamber Engine from Low to High Load. *Appl. Energy Combust. Sci.* **2023**, *15*, No. 100192.